Studying Porosity Effect on Sound Transmission Loss for Firewall Insulator Design

Sajjad BEIGMORADI
AVL Powertrain UK, University of Warwick Science Park, Sovereign Court 2, Sir William Lyons Road, Coventry, UK, sajjad.beigmoradi@avl.com

Abstract: - Noise, vibration, and harshness (NVH) attributes are considered crucial aspects of passenger comfort by automotive manufacturers. Reducing noise and vibration in each of the three sections (source, path, and receiver) can significantly improve passenger comfort. The engine system, in particular, is identified as one of the most challenging vehicle noise sources. Reducing the radiated engine sound in the cabin plays a significant role in decreasing the perceived noise level by occupants. The firewall, as the bulkhead part between the engine and passenger compartment, plays a dominant role in transferring engine noise to the cabin. To prevent this, an optimal design of the firewall structure and related insulator specifications are the most challenging problems from an automotive NVH point of view. Proper design of the firewall insulator requires vast knowledge in material science and acoustics. The composite nature of the insulator, along with many acoustically dependent material parameters, increases the complexity of this component. In this work, the effect of porosity magnitude on the acoustic behavior of the fiber part is investigated. For this purpose, numerical simulation is utilized to achieve significant cost and time reduction. A hybrid finite element-statistical energy analysis (FE-SEA) methodology is applied to simulate the acoustic behavior of materials. The aim is to find the effect of porosity magnitude on the transferred airborne noise in different frequency domains, from low to high range.

Keywords: - NVH, Noise Treatment, Sound Transmission Loss, Hybrid FEA-SEA Method.

1. INTRODUCTION

NVH is considered one of the most difficult challenges in vehicle design. Identifying and mitigating noise sources within the vehicle, whether at the source or along transmission paths to the cabin, involves various techniques explored in numerous studies [1-15]. Using insulators is an effective way to reduce the noise reaching the cabin. Properly designing insulator materials, with a focus on their acoustic properties, is crucial in minimizing the noise levels experienced by passengers. There are many material features that have a direct effect on noise levels in the occupant cabin, such as porosity and tortuosity. Many studies have been conducted to find suitable materials for acoustic packaging and sound insulation in different applications.

Lakshminarayana et al. [16] applied Statistical Energy Analysis to estimate the sound transmission loss (STL) for a typical power plant enclosure. They asserted that this technique can be applied to power plant enclosure design in terms of acoustic characteristics. Saha [17] reviewed the evolution of vehicle sound packages, highlighting key considerations for automotive NVH engineers aiming to optimize sound package treatments.

Lu et al. [18] employed a hybrid FE-SEA model to predict the sound transmission loss (STL) of sound packages at mid-frequencies, accounting for both airborne and structure-borne excitations. They used the FE subsystem to model panels and SEA to model receiving rooms. They evaluated two common sound packages under these conditions. Their findings indicated that foam-backed and septum-backed carpets provided good STL performance under structural excitation between 100-250 Hz, with minor performance variations as core thickness increased. For airborne excitation, both types of carpets had minimal impact on STL in the 100-250 Hz range, though performance improved with greater core thickness.

Kim et al. [19] presented a methodology for predicting the sound transmission loss in extruded aluminum panels. They showed that their FEM method could be used to predict the sound insulation performance of panels during the early stages of development or to recommend improvements. Beigmoradi et al. [20] investigated the impact of various insulator package configurations on radiated noise levels. They examined three parameters for both the inner and outer insulators: two thickness levels for each layer and two types of material. Using design of experiments (DoE), they identified the optimal insulator thickness configuration that maximizes transmission loss. This paper examines the impact of various porosity levels in light glass wool on sound transmission loss, specifically for use as a firewall insulator. Recognized as a key component in transmitting airborne engine noise to the passenger compartment, the firewall is the focus of this detailed analysis. The study investigates how different porosity values influence sound

transmission loss across the firewall insulator at both low and high frequency ranges.

2. BACKGROUND THEORY

2.1. Statistical energy analysis

Statistical Energy Analysis (SEA) considers wave motion in flexural, extensional, and torsional modes. For each wavefield type, all modes within a subsystem that resonate within the analysis frequency band are assumed to share the same average energy. The distribution of these modes is determined by the subsystem's averaged structural or acoustic properties. As a result, the energy of each wavefield in each frequency band is treated as a single degree of freedom, which greatly reduces computational costs compared to deterministic methods. This statistical method involves [21]:

- Ensemble averaging.
- Time averaging, assuming stationary excitation.
- Space averaging over each subsystem.
- Frequency band averaging.

SEA depends on achieving an equilibrium power balance at the subsystem level. For instance, consider a system made up of two single-wavefield subsystems, as illustrated schematically in Figure 1. The power-balance equations for this system are expressed as [22]:

$$P_1 = \omega\eta_1 E_1 + \omega\eta_{12} n_1 \left(\frac{E_1}{n_1} - \frac{E_2}{n_2}\right) \quad (1)$$

$$P_2 = \omega\eta_2 E_2 + \omega\eta_{21} n_2 \left(\frac{E_2}{n_2} - \frac{E_1}{n_1}\right) \quad (2)$$

The center frequency of the analysis band is indicated by ω. The variables P_i denote the time-averaged power inputs from the applied excitations. The symbols E_i, n_i, and ηi represent the energy, modal density, and damping loss factor of the i^{th} wavefield, respectively. The coupling loss factor from the i^{th} wavefield to the j^{th} wavefield is denoted by η_{ij}.

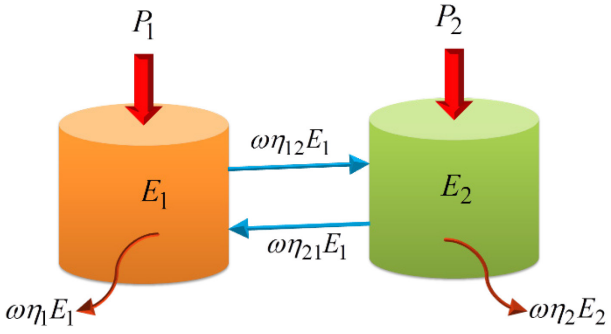

Figure 1. Simple SEA System

The above sketch shows energy flow between subsystems as proportional to:

- The difference in modal energy levels ($\frac{E_i}{n_i}$) of connected subsystems (equivalent to temperature difference in thermal analysis).
- The coupling loss factors (η_{ij}) (equivalent to heat transfer coefficients in thermal analysis).
- The frequency (ω).

For a general system composed of k subsystem wavefields, the power balance equations at each band center frequency, ω, can be presented in matrix form as:

$$\omega CE = P \quad (3)$$

In expression 3, C represents the $k \times k$ coupling loss factor matrix, E is the $k \times 1$ energy vector of unknown wavefield energies, and P is the $k \times 1$ power vector of applied input powers. These terms are generally functions of frequency. The SEA solution process involves constructing and solving the power balance equations at each band-center frequency across the desired frequency range. Typically, the coupling loss factors(CLFs) are influenced by the geometrical properties of the junction, the physical characteristics of the connected subsystems, and the angles at which waves are transmitted relative to the junction. The standard method for analytically evaluating the CLFs is to substitute the connected subsystems with semi-infinite subsystems that share the same junction geometry. This approach is justified because the average input impedances of finite structures tend to align with those of semi-infinite structures when many modes are excited. In the SEA method, specifying boundary conditions for the unconnected portions of subsystem boundaries is unnecessary.

Damping in a structure can occur in various forms, including material damping, damping at joints, and acoustic radiation damping. The damping in an acoustic cavity is determined by the sound absorption characteristics of its boundaries. In SEA, the damping loss factors (DLFs) encompass all forms of damping except acoustic radiation, which is explicitly modeled in terms of power transferred between adjacent subsystems. The stored energy of a wavefield is defined in terms of engineering variables as follows:

$$E = \begin{cases} M\langle v^2 \rangle, & \text{structural wave field} \\ V\langle p^2 \rangle / \rho c^2, & \text{acoustic wave field} \end{cases}$$

Here, M represents the mass of the associated subsystem, Vdenotes the subsystem volume, $\langle v^2 \rangle$ is the space-averaged mean square vibration velocity, $\langle p^2 \rangle$is the space-averaged mean square acoustic

pressure, ρ stands for the fluid density, and c is the speed of sound in the fluid. Once the energies for the different wavefields are calculated, the velocity, acceleration, and sound pressure levels can be derived using this relationship.

2.2. Hybrid FE-SEA method

In the hybrid FE-SEA method, the key step is determining the response of the components designated as SEA subsystems. The remaining parts of the system, referred to as the "deterministic" parts, are modeled using the FE method. If the degrees of freedom for the deterministic parts are labeled q, the governing equations of motion for harmonic vibration at frequency ω will be in the form of equations (4) and (5) [23].

$$D_{tot} q = F + \sum_k F_{rev}^{(k)} \tag{4}$$

$$D_{tot} = D_d + \sum_k D_{dir}^{(k)} \tag{5}$$

The summation is over the number of SEA subsystems in the model, and $D_{dir}^{(k)}$ denotes the direct field dynamic stiffness matrix associated with subsystem k. Additionally, D_d is the dynamic stiffness matrix from the FE model of the deterministic parts of the system, F represents the external forces applied to this part of the system, and $F_{rev}^{(k)}$ signifies the force from the reverberant field in subsystem k, which is not included in $D_{dir}^{(k)}$. The matrix D_{tot} is the dynamic stiffness matrix of the FE model (excluding the SEA subsystem degrees of freedom) when augmented by the direct field dynamic stiffness matrix of each SEA subsystem. It is important to note that equations (4) and (5) are exact; the forces from the SEA subsystems are simply divided into a direct field part, accounted for by $D_{dir}^{(k)}$, and a reverberant part, moved to the right-hand side of equation (4). Shorter and Langley [24] utilized equation (4) to develop the hybrid FE-SEA method.

$$S_{ff}^{(k),rev} \equiv E[F_{rev}^{(k)} . F_{rev}^{(k)*T}] = \left(\frac{4E_k}{\omega \pi n_k} \right) \mathrm{Im}\left\{ D_{dir}^{(k)} \right\} \tag{6}$$

where E_k and n_k represent the (ensemble average) vibrational energy and the modal density of the k^{th} subsystem, respectively. Equation (6) indicates that the cross-spectral matrix of the force exerted by the reverberant field is proportional to the resistive part of the direct field dynamic stiffness matrix, a characteristic of a diffuse field. The response q in equation (4) can be expanded as shown in equation (7) [23].

$$q = q_d + \sum_k q^{(k)} \quad , \; q_d = D_{tot}^{-1} F \, , \; q^{(k)} = D_{tot}^{-1} F_{rev}^{(k)} \tag{7}$$

The time-averaged power input to the direct field of subsystem j is expressed in equation (8) [23].

$$P_{in,j} = (\omega/2) \mathrm{Im}\{q^{*T} D_{dir}^{(j)} q\} = (\omega/2) \sum_k \mathrm{Im}\{D_{dir,rs}^{(j)}\} S_{qq,rs} \tag{8}$$

where the dynamic stiffness matrix is symmetric. If the various contributions $q^{(k)}$ in equation (7) are assumed to be uncorrelated and have a zero mean, then equations (6)-(8) result in

$$P_{in,j} = P_{in,j}^{ext} + \sum_k \omega \eta_{jk} n_j (E_k / n_k) \tag{9}$$

where,

$$P_{in,j}^{ext} = (\omega/2) \sum_k \mathrm{Im}\{D_{dir,rs}^{(j)}\} (D_{tot}^{-1} S_{ff} D_{tot}^{-1*T})_{rs} \tag{10}$$

$$\omega \eta_{jk} n_j = (2/\pi) \sum_k \mathrm{Im}\{D_{dir,rs}^{(j)}\} (D_{tot}^{-1} \mathrm{Im}\{D_{dir}^{(k)}\} D_{tot}^{-1*T})_{rs} \tag{11}$$

Given that the dynamic stiffness matrices are symmetric, equation (11) shows that reciprocity holds, meaning $\eta_{jk} n_j = \eta_{kj} n_k$. As demonstrated below, the terms η_{jk} are equivalent to the coupling loss factors found in SEA.

The power output from the reverberant field in subsystem j can be expressed as the sum of: (i) the power dissipated through damping, (ii) the power transferred to other subsystems, and (iii) the power dissipated in the deterministic system due to the response $q^{(j)}$. Then:

$$P_{out,j} = \omega \eta_j E_j + \sum_k \omega \eta_{kj} n_k (E_j / n_j) + \omega \eta_{d,j} E_j \tag{12}$$

where,

$$\omega \eta_{d,j} = (\omega / 2E_j) \mathrm{Im}\{q^{(j)*T} D_d q^{(j)}\} = \left(\frac{2}{\pi n_j} \right) \sum \mathrm{Im}\{D_{d,rs}\} (D_{tot}^{-1} \mathrm{Im}\{D_{dir}^{(j)}\} D_{tot}^{-1*T})_{rs} \tag{13}$$

Equations (9) and (12) then lead to the following energy balance equation for subsystem j

$$\omega(\eta_j + \eta_{d,j}) E_j + \sum_k \omega \eta_{jk} n_j (E_j / n_j - E_k / n_k) = P_{in,j}^{ext} \tag{14}$$

Additionally, the cross-spectral matrix of the response q can be derived from equations (6) and (7), which yields

$$S_{qq} = D_{tot}^{-1} [S_{ff} + \sum_k \left(\frac{4E_k}{\omega \pi n_k} \right) \mathrm{Im}\{D_{dir}^{(k)}\}] D_{tot}^{-1*T} \tag{15}$$

Equations (14) and (15) constitute the core of the hybrid FE-SEA method. These equations integrate FE and SEA methodologies: equation (14) resembles SEA, but the coupling loss factors η_{jk} and loss factors $\eta_{d,j}$ are computed using the FE model (enhanced by the direct field dynamic stiffness matrices) through equations (11) and (13). Additionally, equation (13) represents standard

deterministic FE analysis, but includes additional forces from the reverberant energies in the subsystems. If there are no SEA subsystems, the method reverts to purely FE analysis.

The acoustic insulation capability of the structures can be estimated by defining the sound transmission loss (STL) based on equation (16) [25].

$$STL(\gamma, f) = 10 \log \frac{P_{in}(\gamma, f)}{P_{out}(\gamma, f)} \quad (16)$$

where: γ is the angle of incidence of the sound wave over the surface of the given partition, f is the frequency of the sound wave being considered, P_{in} is the sound power incident on the source side, P_{out} is the sound power radiated on the opposite side of the partition.

An important aspect to note is that STL depends on the angle of incidence of the sound. The simplest scenario is when acoustic plane waves are normal to the surface. In this case, we can determine the sound transmission loss for normal incidence:

$$STL(f) = 10 \log \frac{P_{in}(f)}{P_{out}(f)} \quad (17)$$

3. SIMULATION PROCEDURE

This research investigates the effect of porosity values ranging from 0.5 to 0.99 in the fiber part of the firewall insulator, which is an applicable range from an acoustic viewpoint [21]. It is assumed that the insulator consists of two layers: a fiber layer and a hard rubber layer. The structure of the insulator layers is shown in Figure 2.

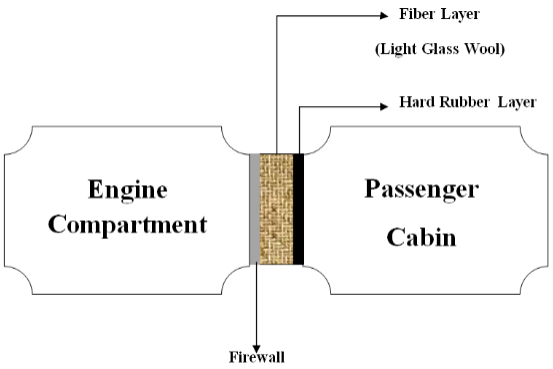

Figure 2. Configuration of insulator layers around firewall

In this study, light glass wool is selected as the fiber layer of the insulator, with a thickness of 30 mm. Its properties are listed in Table 1. Additionally, butyl rubber is used as the second layer because of its excellent damping properties, good thermal stability, and low gas permeability. The properties of butyl rubber are detailed in Table 2.

Table 1. Light glass wool property

Property	Value
Density (Kg/m^3)	16
Flow Resistivity $(N.s/m^4)$	9000
Tortuosity	1

Table 2. Hard rubber property

Property	Value
Thickness (mm)	1
Density (Kg/m^3)	1100
Tensile Module (GPa)	2.3
Hardness (Shore A)	50
Thermal conductivity(W/m.K)	0.15

The porosity magnitude of light glass wool is examined at six levels to achieve maximum sound transmission loss. Simulations are conducted using the hybrid FE-SEA method. The following steps are carried out sequentially:

1- The firewall is modeled as an FE subsystem, connected to a semi-infinite fluid acting as the acoustic medium.

2- A diffuse acoustic field is applied as excitation on the outer side of the firewall in all simulations.

3- Modal analysis of the firewall is performed to determine its dynamic behavior, with the modal results used as input for the SEA simulation.

4- SEA simulation, incorporating boundary conditions and the acoustic diffuse field as the excitation source on the firewall, is conducted, and the resulting data from the acoustic field are collected.

Figure 3 illustrates the configuration of the FE-SEA model.

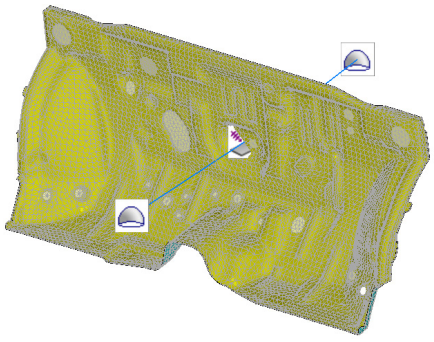

Figure 3. Configuration of FE-SEA model for insulator design

3. MODEL CORRELATION

To ensure accurate simulation results, the primary FE model must be validated. This involves conducting modal analysis of the firewall using both experimental and numerical methods and comparing the results. A free-free boundary condition is used in both numerical and experimental cases for the Body-In-White (BIW). For the experimental test, the BIW was suspended on elastic ropes to create an

unconstrained configuration, representing a free-free boundary condition.

The natural frequency for the suspended BIW rigid motion is less than 1 Hz. Equipment for the modal test includes a laptop with dBFA 4.9 suite software for data acquisition and analysis, a NetdB 12-channel DAQ, charge amplifiers, ICP and charge accelerometers, a force cell, and both a hammer and shaker for modal testing. After comparing the shaker and hammer, the hammer was selected for testing. Generally, the shaker is better for testing the overall structure dynamics (such as flexural and torsional global modes), while the hammer is more effective for exciting local modes and requires fewer transducers. Following the experimental modal test, resonant modes are identified for each panel.

Subsequently, an FE model of the BIW is developed to compare experimental modes with numerical ones. Each part and panel are meshed separately, and a rigid body element (RBE) is used to connect parts and panels, effectively representing body joints such as spot welds.

A mesh dependency check is conducted to determine the optimal element size, balancing calculation cost, time, and accuracy. Initially, a 17 mm element size is chosen based on the maximum frequency limit (10 elements to capture the wavelength at 2000 Hz). However, this size results in the loss of most geometric features, causing significant deviations between the simulation and experimental results, with some modes not captured in the simulation.

To improve accuracy, the element size is refined, striking a balance between model accuracy and simulation cost. A 4 mm element size is identified as suitable, accurately capturing all mode shapes and resonance frequencies. To replicate the experimental test's boundary conditions, no boundary condition is applied to the BIW model. Using a free-free condition, six free rigid modes are observed as the first modes in the simulations.

Figure 4 presents the BIW structure and the corresponding FE model used for the modal test and simulation, respectively.

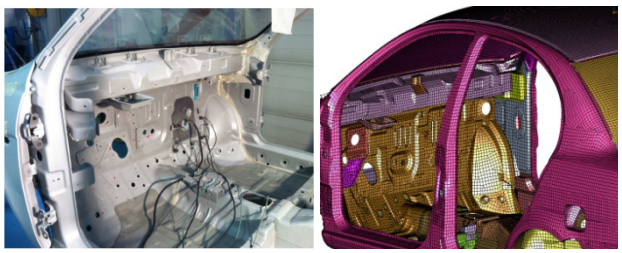

Modal Test for Firewall FEM model of BIW

Figure 4. Firewall setup test and FEM model

Comparing numerical and experimental modal results show good agreement in mode shapes and frequency magnitudes. As a matter of fact, all mode shapes anticipated by numerical simulations are detected in experimental test as well. Overall deviation between modal analysis and practical test is less than 9%. One of the mode shapes of firewall and its corresponding frequency for experimental modal analysis (EMA) and numerical simulation is demonstrated in figure 5 as a sample. Table 3 represents a comparison between experimental results of natural frequencies and those evaluated through numerical simulation.

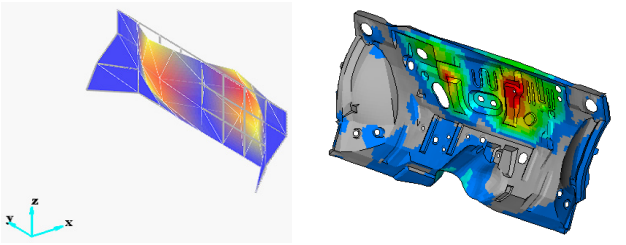

EMA mode shape @148Hz Simulation mode shape@ 152Hz

Figure 5. Comparison numerical and experimental modal result

Table 3. Experimental and numerical frequency modes of firewall

Mode no	Numerical mode (Hz)	Experimental mode(Hz)	Δf (%)
1st	119.88	112.5	6.1
2nd	152.34	148.44	2.5
3rd	221.83	213.67	3.6
4th	338.24	314.84	6.9
5th	374.92	342.86	8.5

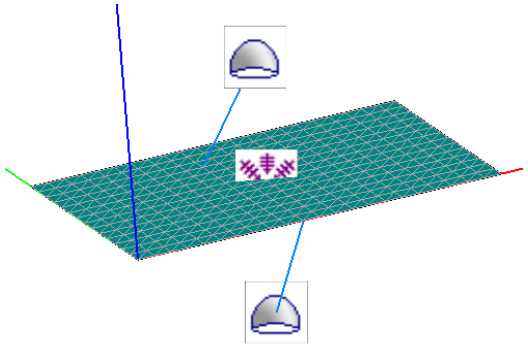

Figure 6. Hybrid FE-SEA configuration-flat panel connected to two SEA SIFs and a SEA DAF

Additionally, to validate the hybrid FE-SEA model, simulation results for a flat panel are compared with analytical results obtained by Sgard et al. [26]. This simulation involves a simply supported flat panel connected to two SEA semi-infinite fluids (SIFs) and excited by an SEA diffuse acoustic field (DAF). The simulation configuration is depicted in Figure 6.

A comparison of the numerical simulation for transmission loss with the results from Sgard et al. [26] reveals good agreement, as illustrated in Figure 7.

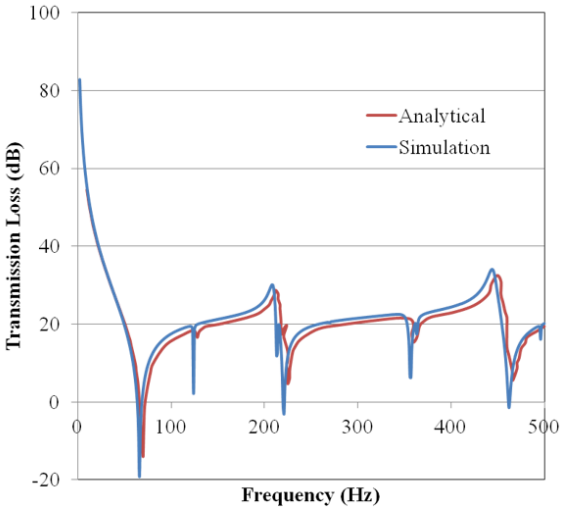

Figure 7. Comparison simulation with analytical [26] results

4. RESULTS AND DISCUSSION

Simulations were performed for six different porosity levels of light glass wool used in the insulator. These levels were chosen based on the results of 12 simulations conducted within the specified porosity range, which showed a consistent trend in the sound transmission loss (STL) curve as porosity increased. The sound transmission loss spectra for the various porosity levels are presented in Figure 8.

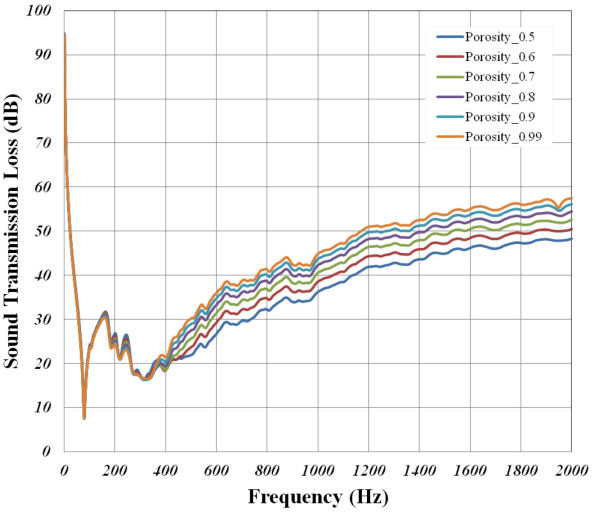

Figure 8. The Sound Transmission Loss (STL) spectra within the 0-2000 Hz range

The STL diagram demonstrates that increasing porosity levels negatively affects sound insulation, especially in the low-frequency range (see Figure 9(a)). The observed trends in the STL curves indicate that raising porosity reduces STL up to around 375 Hz, beyond which the change becomes less noticeable. In other words, reducing porosity in the low-frequency range may enhance sound transmission to the cabin, though the effect is minimal.

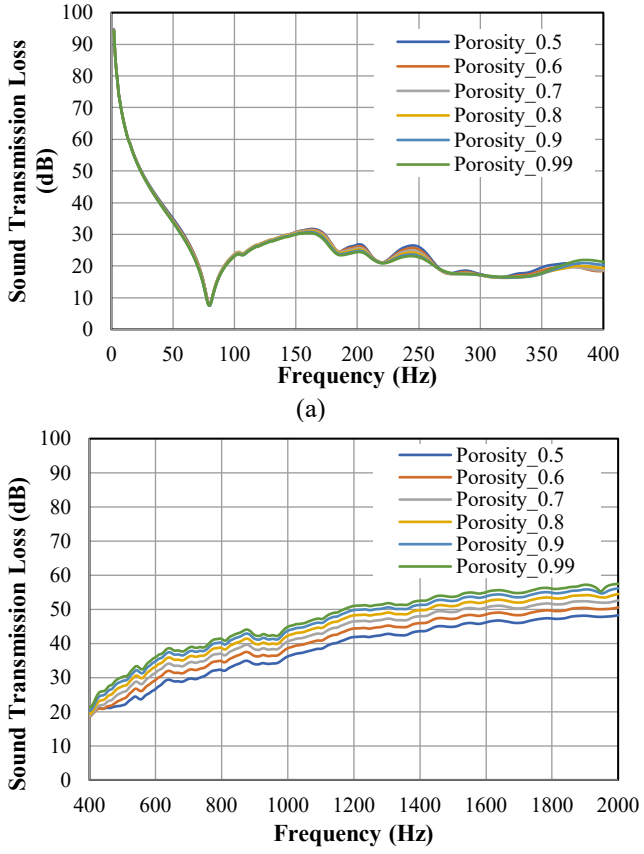

Figure 9. Sound transmission loss (STL) spectra in (a) the low to mid-frequency range and (b) the mid to high frequency range

Figure 9(b) illustrates that increasing porosity significantly improves sound insulation above the 375 Hz threshold. Beyond this frequency, higher porosity in the insulator's structure results in notable enhancements in sound treatment. For example, a porosity level of 0.99 in a lightweight glass wool structure shows an 18% improvement in overall sound transmission loss across the 0-2000 Hz frequency range compared to a porosity of 0.5. This phenomenon can be attributed to three factors. First, higher porosity generates more air pockets within the material, which improves its capacity to absorb sound waves. Second, more porous structures scatter sound waves more effectively, dissipating their energy. Third, the increased surface area in a porous material results in greater frictional losses, converting more sound energy into heat. On the other hand, according to the literature [25], structure-borne noise is dominant at low frequencies (0-200 Hz). The contribution of structure-borne noise decreases in the mid-frequency range as the frequency increases from 200 Hz to 400 Hz. Above 400 Hz, airborne noise becomes the dominant factor in transmission through the passenger cabin. According to Figure 9(a), variations in porosity do not significantly affect sound transmission loss in the low-frequency range where structure-borne noise is predominant. However,

beyond 375 Hz, the influence of porosity becomes more noticeable. This suggests that porosity values have a considerable impact primarily on airborne noise at higher frequencies rather than on structure-borne noise.

Additionally, regardless of the insulator's porosity value, STL generally increases as the frequency rises from 375 Hz to 2000 Hz. For example, the STL for an insulator with a porosity of 0.99 increases significantly from 21 dB to 57 dB. This trend is consistent across all cases, indicating that the effectiveness of the firewall insulator improves with higher frequencies. In other words, a firewall insulator with higher porosity can play a crucial role in mitigating airborne noise.

5. CONCLUSIONS

This work investigates the effect of fiber porosity on sound transmission loss (STL) across a broad frequency range in a firewall insulator. Numerical simulations were conducted to save time and reduce costs. The results indicate that porosity does not significantly impact STL in the low-frequency range (0-375 Hz). However, as the frequency increases beyond 375 Hz, the effect of porosity on STL becomes more pronounced. For frequencies above 375 Hz, higher porosity values lead to increased STL in the insulator. Therefore, while increasing porosity is not an effective solution for structure-borne noise treatment, it plays a significant role in controlling airborne noise in the high-frequency range.

REFERENCES

[1] Bhuwal, A., Kapdi, S., and Jinto, M., Structural Optimization Techniques to Design Light Weight and Low Radiated Noise Components, SAE Int. J. Veh. Dyn., Stab., and NVH 2(3), pp. 203-212, 2018, https://doi.org/10.4271/10-02-03-0013.

[2] Balcı, E., Akalin, O., and Karaca, Ç., Influence of Rib Stiffener Design Parameters on the Noise Radiation of an Engine Block, SAE Int. J. Engines 12(2), pp. 175-184, 2019, https://doi.org/10.4271/03-12-02-0013.

[3] Jahani, K., Beigmoradi, S., Ramezani, A. and Hajabdollahi, H., Panel contribution analysis for a sedan car using numerical simulations, Proceedings of 20th International Congress on Sound & Vibration, 2013.

[4] Beigmoradi, S., and A. Ramezani., Effect of the backlight angle on the aero-acoustics of the C-Pillar., Int. Review on Modelling and Simulations 6, no. 3 (2013), pp. 988-993.

[5] Qatu, Mohamad S., Recent research on vehicle noise and vibration, International Journal of Vehicle Noise and Vibration 8, no. 4 (2012), pp. 289-301.

[6] Wang X., Vehicle noise and vibration refinement, Elsevier; 2010 Mar 12.

[7] Beigmoradi, S., Aerodynamic Drag and Noise Minimization of Rear End Parameters in a Simplified Car Model Utilizing Robust Parameter Design Method, SAE Technical Paper 2015-01-1360, 2015, https://doi.org/10.4271/2015-01-1360.

[8] Moroncini, A., L. Cremers, and Niccolo Baldanzini. Car body concept modeling for NVH optimization in the early design phase at BMW: A critical review and new advanced solutions, Proceedings of the International Conference on Noise and Vibration Engineering, pp. 3809-3823. 2012.

[9] Lu, X. and Ma, J., Development of an Optimization Process for Engine NVH Performance, SAE Technical Paper 2015-01-2292, 2015, https://doi.org/10.4271/2015-01-2292.

[10] Kurian, A., Kunde, S., THAKUR, S., and Wagh, S., Powertrain Optimization Strategy for Downsizing and NVH Refinement, SAE Technical Paper 2022-28-0112, 2022, https://doi.org/10.4271/2022-28-0112.

[11] Beigmoradi, S., Low-Frequency Noise Transfer Path Identification Study for Engine Sub-Frame Utilizing Numerical Simulation, SAE Technical Paper 2015-01-2361, 2015, https://doi.org/10.4271/2015-01-2361.

[12] Fard, M. and Liu, Z., Automotive Body Concept Modeling Method for the NVH Performance Optimization, SAE Technical Paper 2015-01-0012, 2015, https://doi.org/10.4271/2015-01-0012.

[13] Ronzio, F. and Courtois, T., The Use of Trim FE Simulations in Body NVH Design Optimization, SAE Technical Paper 2016-01-1780, 2016, https://doi.org/10.4271/2016-01-1780.

[14] Minervini, D. and Brughmans, M., Efficient Conceptual Tire Model and Parameter Identification for NVH Applications, SAE Technical Paper 2021-01-0937, 2021, https://doi.org/10.4271/2021-01-0937.

[15] Beigmoradi, S., and VAHDATI, M., Enhancement of Vibration Characteristics of an Air Filter Box Utilizing Numerical Analysis, Romanian Journal of Acoustics and Vibration 17, no. 2 (2020): 85-90.

[16] Lakshminarayana, R, Richard, L. L., Umamaheswari, J., Lakshminarayana, H.V., Prediction of Sound Transmission Loss for Power Plant Enclosures Using Statistical Energy Analysis, *SASTECH*. 5(1): 67-69, 2005.

[17] Saha, P., Developing Vehicle Sound Packages, *Sound & Vibration.* 45(10): 10-13, 2011.

[18] Lu, Z., Hao, Z., Zheng,X., Yang, J., Research on the Insertion Loss of Sound Package under Structure-borne and Airborne Excitation in Mid-frequency Using Hybrid FE-SEA Method, *Journal of Computational Information Systems*. 7(4): 1190-1197, 2011

[19] Kim, K., Lee, J., and Kim, D., A Study on the Vibroacoustic Analysis of Aluminum Extrusion Structures, *Computer-Aided Design & Applications*, PACE (2): 1-8, 2012.

[20] Beigmoradi, S., Jahani, K., and Hajabdollahi, H., Investigating the transmission loss effect via optimizing the insulator package on vehicle's firewall, Proceedings of Meetings on Acoustics -Acoustical Society of America. 19, 2013, DOI: 10.1121/1.4801013

[21] User's Guide, Theory & QA, VA One 2012 Foam Module Doc, 2012.

[22] Burroughs, Courtney B., Raymond W. Fischer, and Fred R. Kern., An introduction to statistical energy analysis, The Journal of the Acoustical Society of America 101.4 (1997), pp. 1779-1789.

[23] Langley, R.S., Vibration and stress analysis in the presence of structural Uncertainty, Journal of Physics: Conference Series, 181 2009, doi:10.1088/1742-6596/181/1/012001

[24] Shorter P.J., Langley, R.S., On the reciprocity relationship between direct field radiation and diffuse reverberant loading, *J. Acou. Soc. Am,* 117, pp. 85-95, *2005.*

[25] Wang, X., Vehicle noise and vibration refinement, Woodhead Publishing Limited, Abington Hall, Granta Park, Great Abington, Cambridge, UK, 2010.

[26] Sgard, F. C., N. Atalla, and J. Nicolas., A numerical model for the low frequency diffuse field sound transmission loss of double-wall sound barriers with elastic porous linings, The Journal of the Acoustical Society of America 108, no. 6 (2000), pp. 2865-2872.